THE JOURNAL OF PHYSICAL CHEMISTRY C

pubs.acs.org/JPCC Article

Nanocluster Growth and Coalescence Modulated by Ligands

Dylan Suvlu, Mohsen Farshad, and Jayendran C. Rasaiah*

Cite This: J. Phys. Chem. C 2020, 124, 17340−17346 Read Online

ACCESS | Metrics & More | Article Recommendations | Supporting Information

ABSTRACT: We describe a model of nanocluster formation that incorporates competition between ligand adsorption and nanocluster growth. Growth occurs through the addition of a metal−ligand complex and coalescence of nanoclusters. The competition between ligands for binding sites on the nanoclusters and growth of the nanoclusters through coalescence creates interesting growth pathways. The patterns are reminiscent of those observed in the synthesis of gold thiolate nanoclusters. For a particular set of rate coefficients, described herein, we observe the formation of a kinetically stable nanocluster that participates in coalescent growth. This determines the size interval of the resulting nanoclusters in the size distribution. The kinetically stable cluster can be tuned by modifying the functional form of the number of surface sites on the nanoclusters, thereby changing the growth pathway and the final sizes of the clusters.

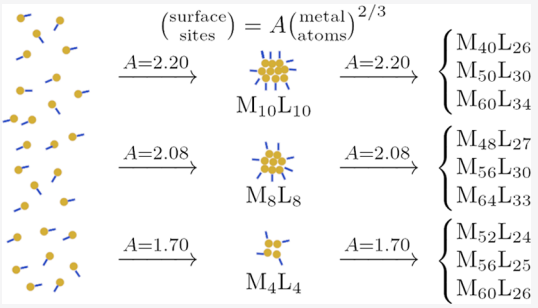

1. INTRODUCTION

Nanoclusters (NCs), defined as clusters of metal atoms less than 2 nm in diameter,[1] contain unique properties with applications in catalysis,[2−6] bioimaging and sensing,[7−10] and medical therapies.[11] The small sizes of NCs present many synthetic challenges.[1] The primary challenge is NCs are metastable since thermodynamic stability increases with particle size.[12] Therefore, successful synthesis of NCs requires precise control over experimental conditions, often utilizing ligands to trap NCs in a metastable state,[6] sometimes referred to as colloidal stability.[13]

Synthesis of NCs generally proceeds through two routes: "bottom-up" and "top-down." In the bottom-up approach, metal ions are reduced to zero or monovalent metal atoms, often in aqueous solution in the presence of ligands, which then proceed to grow and form NCs and nanoparticles. Using this approach, atomically precise NCs have been synthesized with thiolate-protected gold and silver nanoclusters serving as model systems.[1−3,6,14] For example, a typical synthesis procedure for gold NCs consists of the following: (1) mixing of Au(III) salt (e.g., $AuCl_4^-$) with thiol ligands (H-SR) followed by partial reduction to form polymeric complexes of Au(I)-thiol and (2) addition of $NaBH_4$ to reduce Au(I) to Au(0). In both steps, the reagent mixed with Au is in excess. The thiol-to-gold ratio is typically 3:1 or greater, and the $NaBH_4$/Au mole ratio is often 10:1 or more. Under these conditions, and with other synthetic procedures, NCs such as $Au_{15}(SG)_{13}$, $Au_{18}(SG)_{14}$, and $Au_{25}(SG)_{18}$ have been synthesized and studied.[3,14] Despite the remarkable progress in synthesis methodologies and analytical techniques, many questions remain about the formation process and chemistry of thiolate-protected NCs. What is the role of ligands in preventing runaway NC growth? How does the surface chemistry of the NC contribute to the stability of the NC? Advances in microfluidic technology may help to answer some of these questions.[15]

Theoretical models are also leading to an improved understanding.[16−20] Among the many approaches to modeling nanoparticle formation, kinetic rate equations (KREs)[16,18−21] have shown that size focusing is possible in a purely reaction-limited regime.[16] Further, KREs model the evolution of nanoparticle nucleation and growth beginning at the formation of zero-valent metal atoms (monomers) and have an advantage in describing the early stages of NC formation. However, the existing KRE models are limited for two reasons: (1) assumptions from classical nucleation theory (CNT) are incorporated[16,20] and (2) a coalescent growth mechanism is lacking.[16,19−21]

Experiments indicate that CNT fails to correctly describe NC formation[13,22,23] or at least requires modifications to do so.[24] In many experiments, the failure of CNT is demonstrated by the observation of prenucleation clusters—clusters considered too small by CNT to be stable in solution.[25] For strongly associating systems (such as Ir, Au, Ag, etc.), it has been argued that the concept of a critical nucleus from CNT does not apply.[13,18] Therefore, the assumption of a large critical nucleus composed of tens of metal atoms in theoretical models is questionable, especially since experiments indicate that the critical nucleus is just one or two monomers in

Received: May 18, 2020
Revised: July 13, 2020
Published: July 16, 2020

https://dx.doi.org/10.1021/acs.jpcc.0c04459
J. Phys. Chem. C 2020, 124, 17340−17346

strongly associating systems.[18,26,27] Coalescent growth is an important growth mechanism for nanoparticles[13,17,28−32] but was not included in other ligand-mediated growth models,[19−21] including our own.[21]

Here, we have developed a kinetic model of ligand-mediated NC formation, building on previous studies[20,21] by incorporating a coalescent growth pathway and excluding the assumption of a critical nucleus from CNT. The model demonstrates time evolution of a particulate size distribution of NCs where growth proceeds in multiples of a kinetically stable cluster. The size of the kinetically stable NCs can be tuned by modulating the functional form of the number of surface sites as a function of the size of the clusters. Thus, the growth pathway of the NCs can be modified as desired by changing the expression for the surface sites on the clusters. The model also demonstrates how the sizes of NCs are sensitive to the competition between ligand adsorption and monomer addition and coalescence. Our results will be of interest to experimentalists synthesizing NCs and researchers designing synthetic protocols.

2. METHODS

Our model is composed of the following elementary steps. A monovalent metal atom is reduced with rate coefficient k_p (eq 1a). In experiments, the reducing agent is often present in excess; therefore, we model reduction as a first-order reaction. After being reduced, the neutral metal atom can bind/unbind with a ligand with rate coefficients k_b/k_{ub} (eq 1b). A dimer can form through the association of bare metal atoms (eq 1c) or through metal atoms bound to a ligand (eqs 1d and 1e) to form a cluster of metal atoms denoted by $C_{i,j} = M_iL_j$. We denote the rate coefficient for dimer formation k_n, and for simplicity, we assume that each reaction in eqs 1c−1e occurs with the same k_n. Subsequently, cluster growth occurs through the addition of a metal−ligand complex (eq 1f) or a bare metal atom (eq 1g). Growth must compete with ligand association to an NC with i metal atoms and j adsorbed ligands (eq 1h) for a limited number of surface sites $N_s(i)$ on the NCs. Finally, two clusters containing i and k metal atoms and j and l ligands, respectively, may coalesce to form a larger cluster composed of $i + k$ metal atoms and $j + l$ ligands. We place additional constraints on coalescent growth such that $i + k$ must always be less than i_{max} (the maximum size of the NCs in the model) and $j + l$ must always be less than $N_s(i + k)$ (the available number of surface sites on a cluster with $i + k$ metal atoms).

$$M^+ \xrightarrow{k_p} M \tag{1a}$$

$$M + L \underset{k_{ub}}{\overset{k_b}{\rightleftharpoons}} ML \tag{1b}$$

$$M + M \xrightarrow{k_n} C_{2,0} \tag{1c}$$

$$M + ML \xrightarrow{k_n} C_{2,1} \tag{1d}$$

$$ML + ML \xrightarrow{k_n} C_{2,2} \tag{1e}$$

$$C_{i,j} + ML \underset{k_{d_{i,j}}}{\overset{k_{g_{i,j}}}{\rightleftharpoons}} C_{i+1,j+1} \tag{1f}$$

$$C_{i,j} + M \underset{k_{d_{i,j}}}{\overset{k_{g_{i,j}}}{\rightleftharpoons}} C_{i+1,j} \tag{1g}$$

$$C_{i,j} + L \underset{k_{e_{i,j}}}{\overset{k_{a_{i,j}}}{\rightleftharpoons}} C_{i,j+1}$$

$$C_{i,j} + C_{k,l} \xrightarrow{k_{c_{i,k}}} C_{i+k,j+l} \tag{1h}$$

$$\text{if } i + k \le i_{max};\ j + l \le N_s(i + k)$$

$$\forall\ i \ge 2,\ \forall\ i, j \in \mathbb{N} \tag{1i}$$

The rate coefficients for growth $k_{g_{i,j}}$, ligand association $k_{a_{i,j}}$, and coalescence $k_{c_{i,j}}$ depend on the fraction of available surface sites on a cluster with i metal atoms (eqs 2−4). In contrast, the rate coefficients for dissociation $k_{d_{i,j}}$ and ligand elimination $k_{e_{i,j}}$ depend on the fraction of surface sites that are occupied by ligands (eqs 5 and 6). To model the number of surface sites on a cluster of size i, we use the expression $N_s(i) = [2.08i^{2/3}]$ where the brackets round to the nearest integer. The factor 2.08 originates from a fit to experimental data on gold thiolate NCs.[33]

$$k_{g_{i,j}} = k_g\left(1.0 - \frac{j}{N_s(i)}\right) \tag{2}$$

$$k_{a_{i,j}} = k_a\left(1.0 - \frac{j}{N_s(i)}\right) \tag{3}$$

$$k_{c_{i,k}} = k_c\left(1.0 - \frac{j}{N_s(i)}\right)\left(1.0 - \frac{l}{N_s(k)}\right) \tag{4}$$

$$k_{d_{i,j}} = k_d\frac{j}{N_s(i)} \tag{5}$$

$$k_{e_{i,j}} = k_e\frac{j}{N_s(i)} \tag{6}$$

From the above reaction scheme, rate equations for each species can be derived. Next, we provide the rate equation for $C_{i,j}$ (eq 7). The brackets indicate molarity and the factor 1/4 in the last term modeling coalescent growth avoids overcounting the possible combinations of clusters. The equations are solved using the differential equation package in Julia.[34,35]

$$\begin{aligned}\frac{d}{dt}[C_{i,j}] &= k_{g_{i-1,j-1}}[ML][C_{i-1,j-1}] - k_{g_{i,j}}[ML][C_{i,j}]\\ &+ k_{d_{i+1,j+1}}[C_{i+1,j+1}] - k_{d_{i,j}}[C_{i,j}]\\ &+ k_{g_{i-1,j}}[M][C_{i-1,j}] - k_{g_{i,j}}[M][C_{i,j}]\\ &+ k_{d_{i+1,j}}[C_{i+1,j}] - k_{d_{i,j}}[C_{i,j}]\\ &+ k_{a_{i,j-1}}[L][C_{i,j-1}] - k_{a_{i,j}}[L][C_{i,j}]\\ &+ k_{e_{i,j+1}}[C_{i,j+1}] - k_{e_{i,j}}[C_{i,j}]\\ &- \sum_{k=2}\sum_{l=0} k_{c_{i,k}}[C_{i,j}][C_{k,l}]\\ &+ \frac{1}{4}\sum_{i=w+y}\sum_{j=x+z} k_{c_{w,y}}[C_{w,x}][C_{y,z}]\end{aligned}$$

$$\forall\ i \ge 3,\ \forall\ i, j \in \mathbb{N} \tag{7}$$

https://dx.doi.org/10.1021/acs.jpcc.0c04459
J. Phys. Chem. C 2020, 124, 17340−17346

The indices w, x, y, and z in eq 7 are dummy indices. Table 1 provides a summary of the rate coefficients used in the model. For all of the following results, we set $i_{max} = 68$ and the rate coefficients $k_{ub} = 10^{-7}$ s^{-1} and $k_d = 10^{-9}$ s^{-1}.

Table 1. Summary of Model Parameters

reaction	parameter
reduction	k_p
ligand binding/unbinding	k_b/k_{ub}
dimer formation	k_n
monomer growth/dissociation	k_g/k_d
ligand association/elimination	k_a/k_e
coalescent growth	k_c

The full system of ordinary differential equations are provided in the Supporting Information. The number of ODEs n_{eqns} is approximately equal to $n_{eqns} \approx i_{max} + \sum_i^{i_{max}} N_s(i)$. If $i_{max} = 68$ and $N_s(i) = [2.08i^{(2/3)}]$, then $n_{eqns} \approx 1500$. In this case, a single calculation takes approximately 5 h on a single Intel Skylake processor. If $i_{max} = 500$, then $n_{eqns} \approx 40{,}000$. The system becomes prohibitively large as i_{max} increases. To solve the equations, we used the radau solver from the Julia (v1.1.1) differential equation package (v6.9.0) with the absolute and relative tolerances set to 1.0×10^{-10}. The package ODEInterfaceDiffEq (v3.5.0) was used to interface to the radau solver. The equations were solved for a time span of 1.0×10^6 s. Equations for $[\bar{C}_2]$, $[C_{tot}]$, D_{avg}, and number density ρ_i are provided below. The diameters of the NCs are calculated according to a method developed elsewhere,[20] where $D_i = D_M(i/0.45)^{1/3}$ and D_M is the diameter of a monomeric unit, which we set to 0.25 nm. The code is available as a Julia package at https://github.com/dsuvlu/NanoclusterModeler.jl. Additional details about the methods can be found in the Supporting Information.

$$[\bar{C}_i] = \sum_j [C_{i,j}] \tag{8}$$

$$[C_{tot}] = \sum_i \sum_j [C_{i,j}] \tag{9}$$

$$D_{avg} = \sum_i D_i \rho_i \tag{10}$$

$$\rho_i = [\bar{C}_i]/[C_{tot}] \tag{11}$$

3. RESULTS AND DISCUSSION

Utilizing the model, we investigated ligand-mediated nanocluster formation and growth by systematically varying the rate coefficients and initial concentrations of M^+ and L. For the following results, we set $k_p = 10^3$ s^{-1} and $k_b = 10^5$ M^{-1} s^{-1}. This was motivated by the observation that experiments demonstrating synthesis of NCs are often conducted with a strong reducing agent, such as $NaBH_4$. Furthermore, the metal atoms are often bound to one or more ligands before the addition of the reducing agent to the solution. Therefore, our choices of k_p and k_b ensure fast reduction kinetics and that most of the growth will occur through the addition of a metal−ligand complex to the NCs. Figure 1 outlines four scenarios of the different growth pathways observed.

In scenario (I), the ligand elimination rate k_e from the surface of clusters $C_{i,j}$ is larger than the ligand association rate

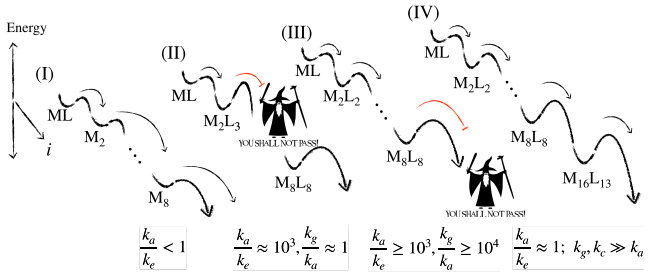

Figure 1. Schematic illustrating some of the different growth pathways observed with the model.

k_a. In this case, there are few ligands on the surface of the NCs to prevent growth and coalescence. Therefore, the clusters grow to large sizes. In scenario (II), the ligand association rate is about 3 orders of magnitude larger than the elimination rate but approximately the same order of magnitude as the growth rate. In this case, the ligands attach to the dimer faster than the dimers can grow. Consequently, growth stops at the dimer. In scenario (III), the ligand association rate is at least 3 orders of magnitude larger than the elimination rate, but the growth rate is at least 4 orders of magnitude larger than the ligand association rate. As a result, the NCs grow until reaching a kinetically stable size of $C_{8,8}$. The size of this kinetically stable cluster is dependent on the expression for the surface sites $N_s(i)$. In scenario (IV), the ligand association and elimination rates are approximately equal; however, the growth and coalescence rates are much greater than the ligand association rate. In this case, the kinetically stable cluster forms during the early stages of growth, and then coalescent growth proceeds in multiples of the kinetically stable cluster. We expand on these observations in the following discussion.

Figure 2 displays data for scenarios (I), (II), and (III). The time evolution of [M], [L], [ML], $[\bar{C}_2]$, $[C_{tot}]$, and average diameter D_{avg} is displayed for $k_a = 10^3$ M^{-1} s^{-1} and for different ligand elimination k_e and growth rates k_g. The NC number density is also plotted as a function of diameter in the penultimate column. Figure 2c displays the number density for scenario (I) where $k_a/k_e < 1$. The rate coefficients are such that growth of the NCs is favorable, but the NCs do not have ligands covering their surfaces to trap the NCs in a metastable state and prevent growth. Therefore, as k_g increases, the NCs grow to large sizes. In contrast, Figure 2a displays the NC number density as a function of diameter for scenarios (II) and (III). In this case, $k_a/k_e \gg 1$, and while $k_g/k_a \approx 1$, growth ceases at the dimer. However, as k_g increases such that $k_g/k_a \gg 1$, growth proceeds to form the kinetically stable cluster $C_{8,8}$ but ceases at this size. Furthermore, the formation of the kinetically stable cluster is sensitive to the ligand elimination rate. Figure 2b displays the NC number density as a function of diameter for $k_e = 10^2$ M^{-1} s^{-1}. In this case, the ligand elimination rate is large enough to allow NC growth beyond the kinetically stable cluster.

Figures 3 and 4 compare the growth pathways of NCs without ($k_c = 0$) and with coalescence ($k_c = 10^3$ M^{-1} s^{-1}), respectively, for a ligand association rate of $k_a = 10^{-3}$ M^{-1} s^{-1}, which is a factor of 10^6 smaller than the ligand association rate in Figure 2. Without coalescent growth, and while $k_a/k_e \geq 1$, the NCs again form the kinetically stable $C_{8,8}$ (Figure 3a,b). However, since k_a is much smaller in this case than that in Figure 2, we do not observe stabilization of the dimer in Figures 3 and 4. Comparing Figure 3b to Figure 4b, where the

https://dx.doi.org/10.1021/acs.jpcc.0c04459
J. Phys. Chem. C 2020, 124, 17340−17346

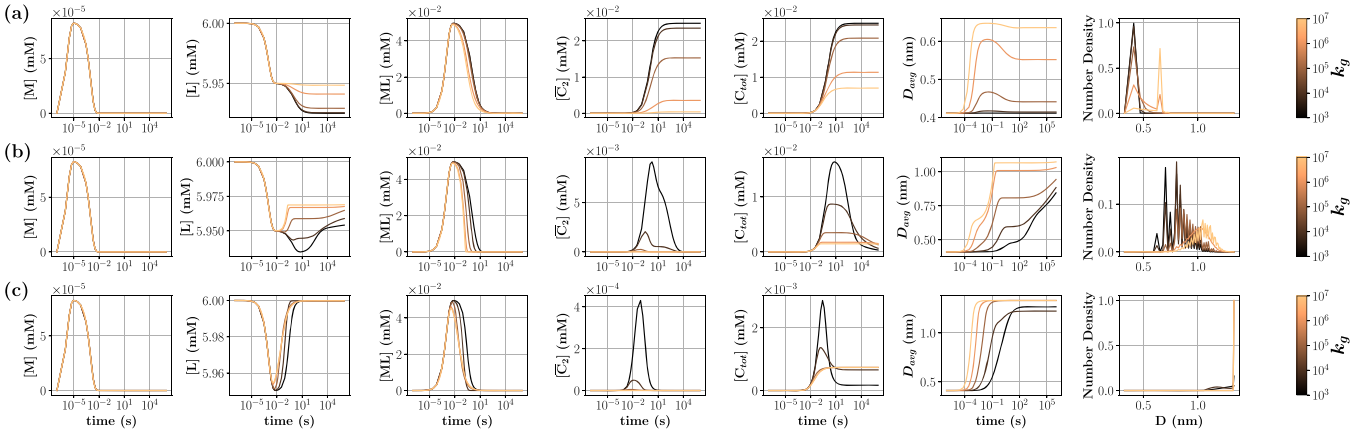

Figure 2. Time evolution for growth with coalescence (k_c = 10^3 M^{-1} s^{-1}), a rapidly associating ligand (k_a = 10^3 M^{-1} s^{-1}), and increasing k_e = (a) 10^{-3}, (b) 10^2, and (c) 10^6 s^{-1}. The number density of NCs as a function of diameter is taken from the last step of the calculation. The remaining rate coefficients were set to k_p = 10^3 s^{-1}, k_b = 10^5 M^{-1} s^{-1}, and k_n = 10^1 M^{-1} s^{-1}. The initial concentrations were [M^+] = 0.05 mM and [L] = 6.00 mM.

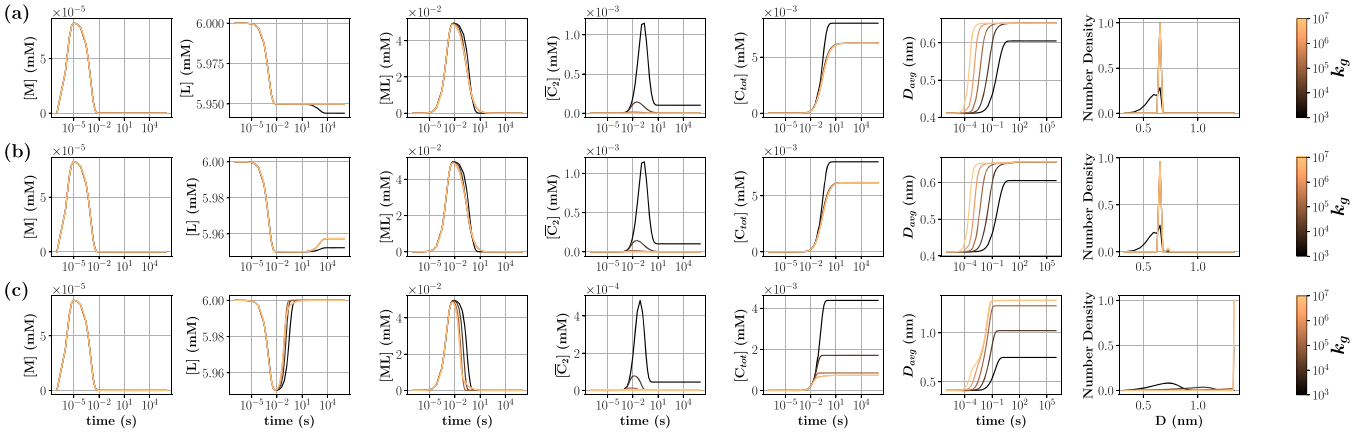

Figure 3. Time evolution for growth without coalescence (k_c = 0), a slowly associating ligand (k_a = 10^{-3} M^{-1} s^{-1}), and increasing k_e = (a) 10^{-6}, (b) 10^{-3}, and (c) 10^3 s^{-1}. The number density of NCs as a function of diameter is taken from the last step of the calculation. The remaining rate coefficients were set to k_p = 10^3 s^{-1}, k_b = 10^5 M^{-1} s^{-1}, and k_n = 10^1 M^{-1} s^{-1}. The initial concentrations were [M^+] = 0.05 mM and [L] = 6.00 mM.

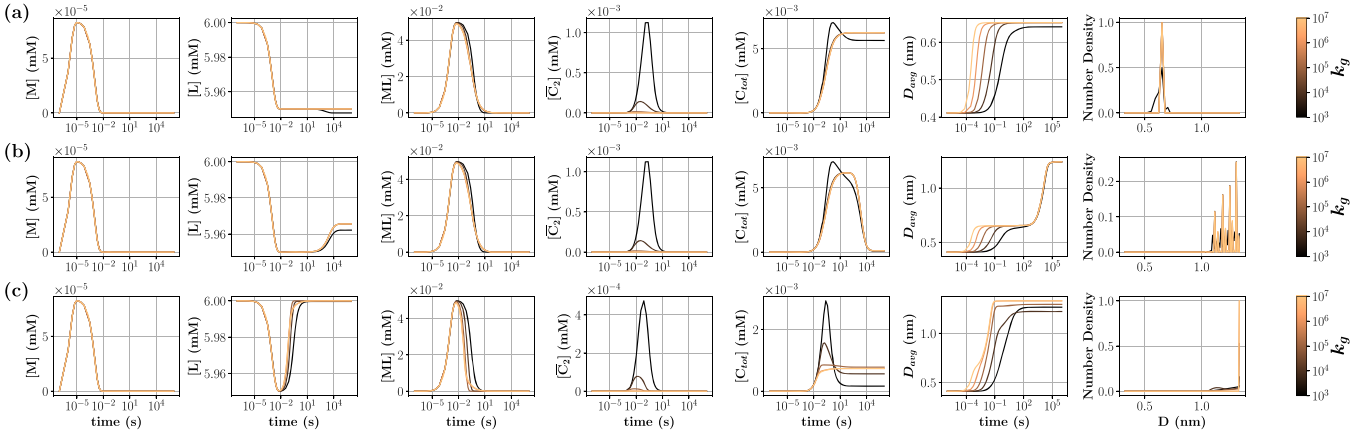

Figure 4. Time evolution for growth with coalescence (k_c = 10^3 M^{-1} s^{-1}), a slowly associating ligand (k_a = 10^{-3} M^{-1} s^{-1}), and increasing k_e = (a) 10^{-6}, (b) 10^{-3}, and (c) 10^3 s^{-1}. The number density of NCs as a function of diameter is taken from the last step of the calculation. The remaining rate coefficients were set to k_p = 10^3 s^{-1}, k_b = 10^5 M^{-1} s^{-1}, and k_n = 10^1 M^{-1} s^{-1}. The initial concentrations were [M^+] = 0.05 mM and [L] = 6.00 mM.

latter incorporates coalescence with k_c = 10^3 M^{-1} s^{-1}, we observe NC growth in factors of the kinetically stable cluster. In this case, k_c, $k_g \gg k_a$ and $k_a/k_e \approx 1$, so that ligand elimination occurs at a rate that allows slow coalescence of the NCs. Under these conditions, the NCs display a particulate size distribution with the spacing determined by the size of the kinetically stable cluster. This is a demonstration of scenario (IV), as discussed earlier. Movie S1 in the Supporting

https://dx.doi.org/10.1021/acs.jpcc.0c04459
J. Phys. Chem. C 2020, 124, 17340−17346

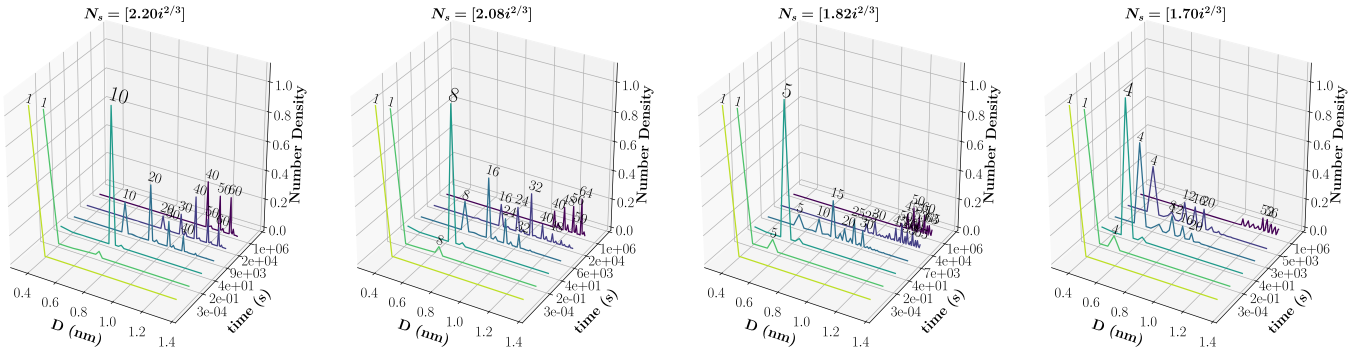

Figure 5. Time evolution of the NC number density as a function of diameter for different N_s. The labels over the peaks indicate the number of metal atoms in the clusters. Note the change in size of the kinetically stable cluster as the functional form of N_s changes.

Information demonstrates the time evolution of the number density and adsorbed ligands for scenarios (I) and (IV). The Supporting Information also contains an expanded collection of results from which we extracted the scenarios discussed here. For example, Figures S15−S18 and Movie S2 display data where the concentration was scaled for different combinations of k_a and k_e.

We also describe the time evolution of the NC size distribution for the rate coefficients used in Figure 4b but with different expressions for $N_s(i)$. Figure 5 illustrates the time evolution of the NC number density as a function of diameter for different expressions of $N_s(i)$. The size of the kinetically stable cluster, as shown in the third plot of the number density in the time evolution, changes from $C_{10,10}$ to $C_{4,4}$ as the scaling factor in $N_s(i)$ changes from the 2.20 to 1.70. This completely changes the results in the size distribution of NCs after coalescent growth is completed. Movie S3 in the Supporting Information illustrates the time evolution of the data displayed in Figure 5. Figure 6 demonstrates that each of the kinetically

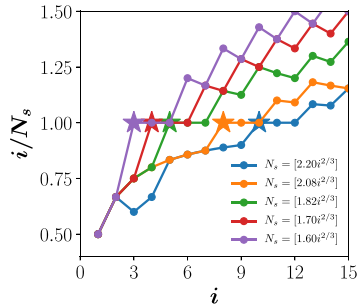

Figure 6. Ratio of the number of metal atoms to the number of surface sites i/N_s as a function of i. The stars indicate the location of the kinetically stable cluster for different functional forms of N_s.

stable clusters occur at $i/N_s(i) = 1.0$ for each expression of $N_s(i)$. This observation can be rationalized in the following way. While $i/N_s(i) < 1.0$, the number of surface sites is greater than the number of metal atoms in the cluster. Therefore, the NCs with $i/N_s(i) < 1.0$ can readily accept a monomer of ML and grow to larger sizes. However, when $i/N_s(i) > 1.0$, the NCs must release a ligand from their surface for additional growth to occur. If the ligand association/elimination kinetics prevent ligand elimination in the short-term then nearly all of the clusters will grow to form the kinetically stable cluster, as illustrated in Figure 5. Coalescent growth will then proceed in factors of the kinetically stable cluster but on a timescale determined by the ligand association/elimination kinetics.

A strength of our model is its unique ability to produce the interesting NC growth patterns observed in Figure 5. These interesting growth pathways originate from competition between NC growth through coalescence and the ligand association/elimination kinetics. We believe that this feature generally describes NC growth when the metal atoms are attached to ligands prior to reduction. However, the interesting growth pathways just described only occur for a particular set of rate coefficients. The rate coefficients are such that dimerization occurs relatively quickly, but not so quickly that all the monomers are depleted from the solution. This allows monomers to attach to the clusters so the clusters grow to larger sizes, eventually forming the kinetically stable cluster. Furthermore, the ligand association rate is sufficiently small such that the ligands do not attach to the growing NCs and prevent growth. These conditions allow the kinetically stable cluster to form. Additionally, the ligand elimination rate is sufficiently slow to allow coalescent growth to occur so that the NCs grow in multiples of the kinetically stable cluster. While this result is exciting because it demonstrates ligand-mediated coalescent growth in a kinetic model for the first time, it also reveals a deficiency in the model.

The model does not ascribe any thermodynamic stability to the NCs except in the sense that the NCs prefer to grow to larger sizes. Thermodynamic products could be incorporated by making select combinations of metal atoms and ligands particularly stable, for example, through the use of super-atom theory.[36,37] An aging process also may be necessary to produce thermodynamic products, which could be done through the incorporation of dis- and comproportionation in the model, both of which have been shown to be important for NC formation.[14,38] We also do not describe further NC interactions between charged species, which can be addressed, for example, using DLVO theory.[13] Additionally, the model presented here does not explicitly account for the differing chemistry of metal atoms on the surface of the nanoclusters compared to the internal structure of the clusters. For example, gold thiolate nanoclusters contain a Au(I)-thiolate motif on the surface with Au(0) contained within the cluster. In the model, the cluster geometry is incorporated implicitly through the expression for the number of binding sites N_s, which originates from a fit to experimental data on gold thiolate clusters. Explicitly distinguishing between surface and internal metal atom chemistry would likely alter the growth dynamics of the model in interesting ways but is unlikely to change our observation of the kinetically stable cluster. The size of the kinetically stable cluster depends on the expression for the

https://dx.doi.org/10.1021/acs.jpcc.0c04459
J. Phys. Chem. C 2020, 124, 17340−17346

number of binding sites on the nanoclusters, which would not change if the model distinguished between surface and internal metal atom chemistry. Lastly, the NCs in Figure 5 only cease to grow because we do not allow coalescent growth beyond i_{max}, the maximum size NC included in the model. The NCs continue to grow to larger sizes with an increase in i_{max}. This could be remedied by using a size-dependent ligand association rate, such that the large NCs prefer to bind ligands more than the small NCs. With this condition, coalescent growth would eventually cease because the NC surfaces would become saturated with ligands.

The growth patterns observed in our model are reminiscent of growth patterns observed in gold thiolate systems[33,39−41] and represent a new development in modeling the formation of gold NCs. For example, Negishi et al.[39] observed the formation of $Au_{10}L_{10}$ where glutathione was the ligand in their system. Similarly, we observe $M_{10}L_{10}$ as the kinetically stable cluster in Figure 5 for $N_s(i) = [2.20i^{2/3}]$. Zeng et al.[40,42] also observed $Au_{10}L_{10}$ as an important precursor in the formation of $Au_{20}L_{16}$, $Au_{28}L_{20}$, $Au_{36}L_{24}$, $Au_{44}L_{28}$, and $Au_{52}L_{32}$ where the ligand was 4-tert-butylbenzenethiol. Furthermore, Dass observed the cluster spacing of Au_4L_4 in the MALDI mass spectra of gold thiolate nanoclusters, suggesting that it was a kinetically stable intermediate in that system.[33] A scaling factor of 1.82 ± 0.33 resulted from a fit of $N_s(i)$ to Au_iL_j. We observe M_5L_5 as the kinetically stable cluster when $N_s(i) = [1.82i^{2/3}]$. However, when $N_s(i) = [1.70i^{2/3}]$, we observe M_4L_4 as the kinetically stable cluster. The scaling factor of 1.70 is within the estimated uncertainty of experimental data.[33] With the improvements suggested above, it may be possible to precisely reproduce these experimental results. However, it is clear from this study that any model attempting to describe nanocluster formation must include coalescent growth and the effects of ligands in preventing the growth process.

4. CONCLUSIONS

We have described a kinetic model of ligand-mediated nanocluster formation. The model demonstrates the relative importance of the single monomer (classical) and coalescent growth pathways. Coalescent growth can occur in factors of a kinetically stable cluster but this growth pathway is very sensitive to ligand association/elimination kinetics to the surface of the NCs. We also showed how the NC growth pathway can be modified by changing the functional form of the surface sites as a function of NC size. Specifically, we observed kinetically stable cluster of sizes $M_{10}L_{10}$, M_8L_8, M_5L_5, and M_4L_4 for scaling factors of 2.20, 2.08, 1.82, and 1.70, respectively, in the expression for the number of binding sites on the NCs. The latter cluster size of M_4L_4 has been observed in the spacing of the MALDI mass spectra of gold thiolate nanoclusters, suggesting that it was the kinetically stable cluster in that system. Our results suggest that the final size distribution of nanoclusters can be altered by changing the number of binding sites on the surfaces of nanoclusters, perhaps by altering the steric hindrance using more or less bulky ligands. These results will be of interest to experimentalists synthesizing nanoclusters.

■ ASSOCIATED CONTENT

Supporting Information

The Supporting Information is available free of charge at https://pubs.acs.org/doi/10.1021/acs.jpcc.0c04459.

Figures S1−S19, full set of equations (PDF)

Movies S1, time evolution of number density and adsorbed ligands for scenarios (I) and (IV) (MP4)

Movie S2, data where the concentration was scaled for different combinations of k_a and k_e (MP4)

Movie S3, time evolution of the data displayed in Figure 5 (MP4)

■ AUTHOR INFORMATION

Corresponding Author

Jayendran C. Rasaiah − *Department of Chemistry, University of Maine, Orono, Maine 04469, United States;* orcid.org/0000-0002-4453-7438; Email: rasaiah@maine.edu

Authors

Dylan Suvlu − *Department of Chemistry, University of Maine, Orono, Maine 04469, United States;* orcid.org/0000-0003-3216-1338

Mohsen Farshad − *Department of Chemistry, University of Maine, Orono, Maine 04469, United States;* orcid.org/0000-0001-5095-4361

Complete contact information is available at: https://pubs.acs.org/10.1021/acs.jpcc.0c04459

Notes

The authors declare no competing financial interest.

■ ACKNOWLEDGMENTS

We thank Stephen Cousins of the Advanced Computing Group at the University of Maine for his continued support and technical assistance. We also thank Rongchao Jin for helpful comments and bringing our attention to refs 40 and 42.

■ REFERENCES

(1) Lu, Y.; Chen, W. Sub-Nanometre Sized Metal Clusters: From Synthetic Challenges to the Unique Property Discoveries. *Chem. Soc. Rev.* **2012**, *41*, 3594−3623.

(2) Chakraborty, I.; Pradeep, T. Atomically Precise Clusters of Noble Metals: Emerging Link between Atoms and Nanoparticles. *Chem. Rev.* **2017**, *117*, 8208−8271.

(3) Jin, R.; Zeng, C.; Zhou, M.; Chen, Y. Atomically Precise Colloidal Metal Nanoclusters and Nanoparticles: Fundamentals and Opportunities. *Chem. Rev.* **2016**, *116*, 10346−10413.

(4) Liu, L.; Corma, A. Metal Catalysts for Heterogeneous Catalysis: From Single Atoms to Nanoclusters and Nanoparticles. *Chem. Rev.* **2018**, *118*, 4981−5079.

(5) Zhao, S.; Jin, R.; Jin, R. Opportunities and Challenges in CO_2 Reduction by Gold and Silver-Based Electrocatalysts: From Bulk Metals to Nanoparticles and Atomically Precise Nanoclusters. *ACS Energy Lett.* **2018**, *3*, 452−462.

(6) Fang, J.; Zhang, B.; Yao, Q.; Yang, Y.; Xie, J.; Yan, N. Recent Advances in the Synthesis and Catalytic Applications of Ligand-Protected, Atomically Precise Metal Nanoclusters. *Coord. Chem. Rev.* **2016**, *322*, 1−29.

(7) Tao, Y.; Li, M.; Ren, J.; Qu, X. Metal Nanoclusters: Novel Probes for Diagnostic and Therapeutic Applications. *Chem. Soc. Rev.* **2015**, *44*, 8636−8663.

(8) Zhang, L.; Wang, E. Metal Nanoclusters: New Fluorescent Probes for Sensors and Bioimaging. *Nano Today* **2014**, *9*, 132−157.

(9) Shang, L.; Dong, S.; Nienhaus, G. U. Ultra-Small Fluorescent Metal Nanoclusters: Synthesis and Biological Applications. *Nano Today* **2011**, *6*, 401−418.

(10) Lee, T.-H.; Gonzalez, J. I.; Zheng, J.; Dickson, R. M. Single-Molecule Optoelectronics. *Acc. Chem. Res.* **2005**, *38*, 534−541.

(11) Webb, J. A.; Bardhan, R. Emerging Advances in Nanomedicine with Engineered Gold Nanostructures. *Nanoscale* **2014**, *6*, 2502.
(12) Thanh, N. T. K.; Maclean, N.; Mahiddine, S. Mechanisms of Nucleation and Growth of Nanoparticles in Solution. *Chem. Rev.* **2014**, *114*, 7610−7630.
(13) Polte, J. Fundamental Growth Principles of Colloidal Metal Nanoparticles − A New Perspective. *CrystEngComm* **2015**, *17*, 6809−6830.
(14) Yao, Q.; Chen, T.; Yuan, X.; Xie, J. Toward Total Synthesis of Thiolate-Protected Metal Nanoclusters. *Acc. Chem. Res.* **2018**, *51*, 1338−1348.
(15) Lignos, I.; Maceiczyk, R.; deMello, A. J. Microfluidic Technology: Uncovering the Mechanisms of Nanocrystal Nucleation and Growth. *Acc. Chem. Res.* **2017**, *50*, 1248−1257.
(16) Rempel, J. Y.; Bawendi, M. G.; Jensen, K. F. Insights Into the Kinetics of Semicon ductor Nanocrystal Nucleation and Growth. *J. Am. Chem. Soc.* **2009**, *131*, 4479−4489.
(17) Wang, F.; Richards, V. N.; Shields, S. P.; Buhro, W. E. Kinetics and Mechanisms of Aggregative Nanocrystal Growth. *Chem. Mater.* **2013**, *26*, 5−21.
(18) Laxson, W. W.; Finke, R. G. Nucleation is Second Order: An Apparent Kinetically Effective Nucleus of Two for Ir(0)n Nanoparticle Formation from [(1,5COD)IrI·P2W15Nb3O62] 8−Plus Hydrogen. *J. Am. Chem. Soc.* **2014**, *136*, 17601−17615.
(19) Mozaffari, S.; Li, W.; Thompson, C.; Ivanov, S.; Seifert, S.; Lee, B.; Kovarik, L.; Karim, A. M. Colloidal Nanoparticle Size Control: Experimental and Kinetic Modeling Investigation of the Ligand-Metal Binding Role in Controlling the Nucleation and Growth Kinetics. *Nanoscale* **2017**, *9*, 13772−13785.
(20) Lazzari, S.; Theiler, P. M.; Shen, Y.; Coley, C. W.; Stemmer, A.; Jensen, K. F. Ligand Mediated Nanocrystal Growth. *Langmuir* **2018**, *34*, 3307−3315.
(21) Farshad, M.; Suvlu, D.; Rasaiah, J. C. Ligand-Mediated Nanocluster Formation with Classical and Autocatalytic Growth. *J. Phys. Chem. C* **2019**, *123*, 29954−29963.
(22) Lee, J.; Yang, J.; Kwon, S. G.; Hyeon, T. Nonclassical Nucleation and Growth of Inorganic Nanoparticles. *Nat. Rev. Mater.* **2016**, *1*, 16034.
(23) You, H.; Fang, J. Particle-Mediated Nucleation and Growth of Solution-Synthesized Metal Nanocrystals: A New Story Beyond the LaMer Curve. *Nano Today* **2016**, *11*, 145−167.
(24) Zahn, D. Thermodynamics and Kinetics of Prenucleation Clusters, Classical and Non Classical Nucleation. *ChemPhysChem* **2015**, *16*, 2069−2075.
(25) Gebauer, D.; Kellermeier, M.; Gale, J. D.; Bergström, L.; Cölfen, H. Pre-Nucleation Clusters as Solute Precursors in Crystallisation. *Chem. Soc. Rev* **2014**, *43*, 2348−2371.
(26) Stamplecoskie, K. G.; Scaiano, J. C. Kinetics of the Formation of Silver Dimers: Early Stages in the Formation of Silver Nanoparticles. *J. Am. Chem. Soc.* **2011**, *133*, 3913−3920.
(27) Völkle, C. M.; Gebauer, D.; Cölfen, H. High-Resolution Insights into the Early Stages of Silver Nucleation and Growth. *Faraday Discuss.* **2015**, *179*, 59−77.
(28) Zheng, H.; Smith, R. K.; Jun, Y.-w.; Kisielowski, C.; Dahmen, U.; Alivisatos, A. P. Observation of Single Colloidal Platinum Nanocrystal Growth Trajectories. *Science* **2009**, *324*, 1309−1312.
(29) Takesue, M.; Tomura, T.; Yamada, M.; Hata, K.; Kuwamoto, S.; Yonezawa, T. Size of Elementary Clusters and Process Period in Silver Nanoparticle Formation. *J. Am. Chem. Soc.* **2011**, *133*, 14164−14167.
(30) Finney, E. E.; Finke, R. G. The Four-Step, Double-Autocatalytic Mechanism for Transition-Metal Nanocluster Nucleation, Growth, and Then Agglomeration: Metal, Ligand, Concentration, Temperature, and Solvent Dependency Studies. *Chem. Mater.* **2008**, *20*, 1956−1970.
(31) Besson, C.; Finney, E. E.; Finke, R. G. Nanocluster Nucleation, Growth, and Then Agglomeration Kinetic and Mechanistic Studies: A More General, Four-Step Mechanism Involving Double Autocatalysis. *Chem. Mater.* **2005**, *17*, 4925−4938.
(32) Besson, C.; Finney, E. E.; Finke, R. G. A Mechanism for Transition-Metal Nanoparticle Self-Assembly. *J. Am. Chem. Soc.* **2005**, *127*, 8179−8184.
(33) Dass, A. Nano-Scaling Law: Geometric Foundation of Thiolated Gold Nanomolecules. *Nanoscale* **2012**, *4*, 2260.
(34) Bezanson, J.; Edelman, A.; Karpinski, S.; Shah, V. B. Julia: A Fresh Approach to Numerical Computing. *SIAM Review* **2017**, *59*, 65−98.
(35) Rackauckas, C.; Nie, Q. DifferentialEquations.jl − A Performant and Feature-Rich Ecosystem for Solving Differential Equations in Julia. *J. Open Res. Softw.* **2017**, *5*.
(36) Aikens, C. M. Electronic Structure of Ligand-Passivated Gold and Silver Nanoclusters. *J. Phys. Chem. Lett.* **2011**, *2*, 99−104.
(37) Walter, M.; Akola, J.; Lopez-Acevedo, O.; Jadzinsky, P. D.; Calero, G.; Ackerson, C. J.; Whetten, R. L.; Grönbeck, H.; Häkkinen, H. A Unified View of Ligand-Protected Gold Clusters as Superatom Complexes. *Proc. Natl. Acad. Sci. U. S. A.* **2008**, *105*, 9157−9162.
(38) Goswami, N.; Yao, Q.; Chen, T.; Xie, J. Mechanistic Exploration and Controlled Syn thesis of Precise Thiolate-Gold Nanoclusters. *Coord. Chem. Rev.* **2016**, *329*, 1−15.
(39) Negishi, Y.; Nobusada, K.; Tsukuda, T. Glutathione-Protected Gold Clusters Revisited: Bridging the Gap between Gold(I)-Thiolate Complexes and Thiolate-Protected Gold Nanocrystals. *J. Am. Chem. Soc.* **2005**, *127*, 5261−5270.
(40) Zeng, C.; Chen, Y.; Iida, K.; Nobusada, K.; Kirschbaum, K.; Lambright, K. J.; Jin, R. Gold Quantum Boxes: On the Periodicities and the Quantum Confinement in the Au_{28}, Au_{36}, Au_{44}, and Au_{52} Magic Series. *J. Am. Chem. Soc.* **2016**, *138*, 3950−3953.
(41) Yao, Q.; Yuan, X.; Fung, V.; Yu, Y.; Leong, D. T.; Jiang, D.-e.; Xie, J. Understanding Seed-Mediated Growth of Gold Nanoclusters at Molecular Level. *Nat. Commun.* **2017**, *8*, 927.
(42) Zeng, C.-j.; Zhou, M.; Gayathri, C.; Gil, R. R.; Sfeir, M. Y.; Jin, R. $Au_{10}(TBBT)_{10}$: The Beginning and the End of Aun(TBBT)m Nanoclusters. *Chin. J. Chem. Phys.* **2018**, *31*, 555−562.

https://dx.doi.org/10.1021/acs.jpcc.0c04459
J. Phys. Chem. C 2020, 124, 17340−17346